*Polish Journal of Chemical Technology, 19, **4**, 65—74, 10.1515/pjct-2017-0069*

Removal of Rhodamine B from aqueous solution by $ZnFe_2O_4$ nanocomposite with magnetic separation performance

Wojciech Konicki[1*], Daniel Siber[2], Urszula Narkiewicz[2]

[1]Maritime University of Szczecin, Department of Environmental Protection, Henryka Pobożnego 11, 70-507 Szczecin, Poland
[2]West Pomeranian University of Technology, Szczecin, Institute of Chemical and Environment Engineering, Faculty of Chemical Technology and Engineering, ul. Pułaskiego 10, Szczecin 70-322, Poland
[*]Corresponding author: e-mail: w.konicki@am.szczecin.pl

Magnetic ZnFe2O4 nanocomposite (ZnFe-NC) was used as an adsorbent for the removal of Rhodamine B (RB) from aqueous solution. The synthesized nanocomposite was characterized by XRD, SEM, HRTEM, BET and FTIR. The effects of various parameters such as initial RB concentration (5–25 mg L^{-1}), pH (3.4–11.1) and temperature (20–60°C) were investigated. The adsorption capacity at equilibrium increased from 5.02 to 9.83 mg g^{-1}, with the increase in the initial concentration of RB from 5 to 25 mg L^{-1} at pH 7.0 and at 20°C. The experimental results indicated that the maximum RB removal could be attained at a solution pH of 4.4 and the adsorption capacity obtained was 6.02 mg g^{-1}. Kinetic adsorption data were analyzed using the pseudo-first-order kinetic model, the pseudo-second-order model and the intraparticle diffusion model. The adsorption kinetics well fitted using a pseudo-second-order kinetic model. The experimental isotherm data were analyzed using two isotherm models, namely, Langmuir and Freundlich. The results revealed that the adsorption behavior of the RB onto ZnFe-NC fitted well with the Langmuir isotherm model. In addition, various thermodynamic parameters, such as standard Gibbs free energy (ΔG^o), enthalpy (ΔH^o) and entropy (ΔS^o) have been calculated.

Keywords: adsorption, Rhodamine B, $ZnFe_2O_4$, kinetics, thermodynamics.

INTRODUCTION

Synthetic dyes are used extensively in the textile, paper, plastic, leather and other industries. At present, there are more than 100 000 dyes available commercially, and over 1 million tons dyes are produced per year, of which 50% are textile dyes. It is estimated that approximately 2% of the dyes produced are discharged directly in aqueous effluent, and 10% is subsequently lost during the coloration proces[1]. The presence of even low concentrations of dyes in water reduces light penetration through the water surface, precluding the photosynthesis of the aqueous flora. Additionally many dyes are carcinogenic, mutagenic and teratogenic and also toxic to human beings, microorganisms, and fish species.

One of the most important dyes within the overall category of dyestuffs is Rhodamine B. Rhodamine B, an important representative of xanthene dyes, is a water-soluble synthetic dye extensively used as a colorant in textile industries and food stuffs, and is also a well--known water tracer fluorescent, which has the property of carcinogenicity, reproductive and developmental toxicity, neurotoxicity, and chronic toxicity towards humans and animals[2]. Therefore, it is very important to remove Rhodamine B and other dangerous dyes from industrial wastewater before being discharged into environment.

There are various methods available for dye removals which include chemical coagulation-flocculation[3, 4], adsorption[5, 6], chemical oxidation[7, 8], photocatalytic degradation[9, 10] and membrane filtration[11, 12]. Amongst the numerous techniques of dye removal, the adsorption process is one of the effective techniques that have been successfully employed for color removal from wastewater. Therefore, many researchers have studied the feasibility of using various types of adsorbents for the removal of Rhodamine B from aqueous solutions. Selvam et al. have studied a removal of Rhodamine B from aqueous solution by adsorption onto sodium montmorillonite clay[13]. Gad and El-Sayed have synthesized an activated carbon from bagasse pith as the adsorbent for the removal of Rhodamine B from aqueous solution[14]. Huang et al. have developed a hypercrosslinked polymeric adsorbent for removal of Rhodamine B form aqueous solution[15]. Shah et al. used walnut shells for removal of Rhodamine B from aqueous solutions and wastewater[16]. Liu et al. have prepared the tannic acid functionalized graphene nanocomposite for removal of Rhodamine B from aqueous solution[17]. Khan et al. have studied the removal of Rhodamine B from an aqueous solution by kaolinite[18]. Vijayakumar et al. have studied a removal of Rhodamine B from aqueous solutions by using a low cost natural adsorbent perlite[19].

The adsorption processes for contaminants removal are efficient and promising, but there is one bottle-neck in their application – separation of adsorbent. Using of magnetic adsorbents can help to overcome that barrier. Compared with traditional centrifugation and filtration methods, the magnetic separation method is considered as a quick and effective technique for separating adsorbents from environmental applications. In recent years, several researchers has been interested in magnetic separation of adsorbents in form of magnetic nanocomposites used for removal of dyes from aqueous solutions. Zhang and Kong have synthesized magnetic Fe_3O_4/C core-shell nanoparticles as adsorbents for removal of organic dyes from aqueous solutions[20]. Xie et al. have prepared magnetic halloysite nanotubes/iron oxide composites for the adsorption of Methylene blue, Neutral red and Methyl orange[21]. Singh et al. have developed and characterized a novel magnetic carbon-iron oxide nanocomposite for adsorption of Crystal violet from water[22]. Madrakian et al. used magnetic-modified MWCNT for removal of Crystal violet, Thionine, Janus green B and Methylene blue

from aqueous solutions[23]. Mahmoodi have synthesized and characterized magnetic ferrite nanoparticle-alginate composite as adsorbent for removal of Basic Blue 9, Basic Blue 41 and Basic Red 18 from aqueous solution[24]. Gao et al. have prepared magnetic polymer multi-wall carbon nanotube nanocomposite as adsorbent for removal of anionic azo dyes Orange II, Sunset yellow FCF and Amaranth from aqueous solution[25]. Yao et al. have synthesized magnetic Fe_3O_4@graphene nanocomposite for removal of Methylene blue and Congo red[26]. Wu et al. have synthesized of superparamagnetic graphene-Fe_3O_4 nanocomposite by a facile one-pot solvothermal method for adsorption of Pararosaniline from aqueous solution[27]. Wang et al. have prepared different MFe_2O_4 (M=Mn, Fe, Co, Ni) spinel ferrites nanocrystals synthesized by hydrothermal method for the removal of Congo Red[28]. Ai et al. have synthesized montmorillonite/$CoFe_2O_4$ composite for removal of removal of Methylene blue from aqueous solution[29].

Therefore, it is very interesting to test the capability of magnetic nanocomposites to eliminate dyes from water. Thus, in this work, magnetic $ZnFe_2O_4$ nanocomposite synthesized by a microwave assisted hydrothermal method was used for the removal of Rhodamine B from aqueous solutions. The effect of various experimental parameters such as initial dye concentration, pH and temperature on the adsorption process were evaluated. In addition, the adsorption isotherms, kinetic and thermodynamic analyses were carried out. The Langmuir and Freundlich equations were used to fit the equilibrium data. The experimental kinetic data were analyzed using the Lagergren pseudo-first-order kinetic model, the pseudo-second-order model, and the intraparticle diffusion model. The thermodynamic parameters of the process, such as enthalpy, entropy and the standard Gibbs free energy, were also determined.

MATERIAL AND METHODS

Material

$Zn(NO_3)_2 \cdot 6H_2O$ and $Fe(NO_3)_2 \cdot 4H_2O$ and KOH supplied by Chempur was used for the preparation of sample $ZnFe_2O_4$ nanocomposite. Rhodamine B ($C_{28}H_{31}ClN_2O_3$, molar mass 479.01) supplied by Zachem Barwniki was used as an adsorbate. The chemical structures of Rhodamine B in the cationic and zwitterionic form are shown in Figure 1. All solutions were prepared using deionized water. All the reagents were of analytical grade and used as received without further purification.

Synthesis of ZnFe-NC

ZnFe-NC nanocomposite which are prepared by using a microwave hydrothermal synthesis pressure 3.9 MPa and time 15 min at have been investigated. At first, a mixture of iron and zinc hydroxides was obtained by addition of 2 M solution of KOH to the 20% solution of a proper amount of $Zn(NO_3)_2 \cdot 6H_2O$ and $Fe(NO_3)_2 \cdot 4H_2O$ in water and then treated in a solvothermal microwave reactor. Next the obtained materials were washed with deionized water to remove salt residues. Finally, the materials were dried at 100°C for 24 h.

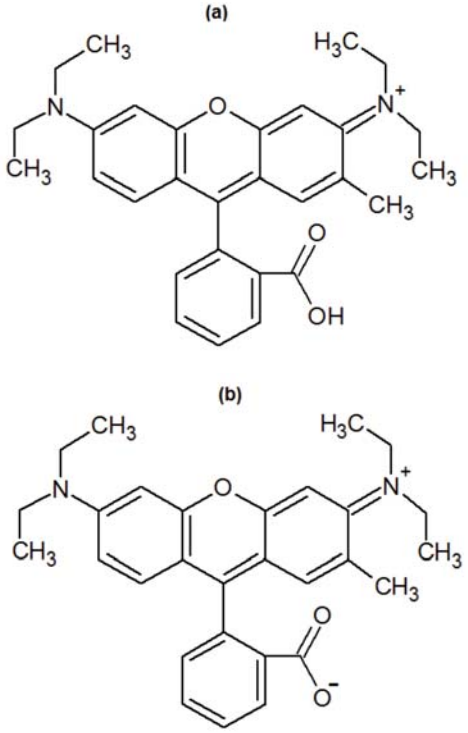

Figure 1. Structures of RB – cationic (a) and zwitterionic (b) form

Characterization methods

The phase composition of the samples was determined using X-ray diffraction (XRD) was conducted on a X'Pert PRO Philips diffractometer using CuKα radiation. The morphology of the ZnFe-NC was examined by scanning electron microscopy SEM Zeiss Supra and high-resolution transmission electron microscope (HRTEM) FEI Tecnai F20 operating at 200 kV. The specific surface area of ZnFe-NC was measured by the BET method, using a Gemini 2360 Micromeritics surface area analyzer. The functional groups of ZnFe-NC were identified by Fourier transform infrared spectroscopy FTIR analysis using a Perkin Elmer Spectrum One FT-IR spectrometer. The point of zero charge pHpzc of ZnFe-NC was determined by the pH drift method[30].

Adsorption experiments

Adsorption experiments were carried out in Erlenmeyer flask, where the solution (200 mL) with an initial dye concentration was placed. Initial concentrations of RB were varied from 5 to 25 mg L^{-1}. The flask with RB solution was sealed and placed in a temperature controlled shaking water bath (Grant OLS26 Aqua Pro, Grant Instruments Ltd) and agitated at a constant speed of 160 rpm. To observe the effect of temperature the experiments were carried out at three different temperatures, i.e., 20, 40 and 60°C. Before mixing with the adsorbent, various pH levels of the solution was adjusted by adding a few drops of diluted hydrochloric acid (0.1 N HCl) or sodium hydroxide (0.1 N NaOH). When the desired temperature was reached, about 30 mg of ZnFe-NC was added into flask. At the end of the equilibrium period 2 ml of aqueous sample was taken from the solution, and the liquid was separated from the adsorbent magnetically. The determination of RB concentration was done spectrophotometrically (GENE-

SYS 10S UV-VIS Spectrometer, Thermo Scientific) at maximum absorbance λ_{max} =554 nm.

The amount of RB adsorbed at equilibrium qe (mg g^{-1}) was calculated by following equation:

$$q_e = \frac{(C_0 - C_e)V}{m} \quad (1)$$

where C_O (mg L^{-1}) is the initial RB concentration, C_e (mg L^{-1}) the RB concentration at equilibrium, V (L) the volume of the solution and m (g) is the mass of the adsorbent.

The procedures of kinetic experiments were identical with those of equilibrium tests. At predetermined moments, aqueous samples were taken from the solution, the liquid was separated from the adsorbent and concentration of RB in solution was determined spectrophotometrically. The amount of RB adsorbed at time t q_t (mg g^{-1}) was calculated by following equation:

$$q_t = \frac{(C_0 - C_t)V}{m} \quad (2)$$

where C_t (mg L^{-1}) the RB concentration at any time t. Each experiment was carried out in duplicate and the average results are presented. The kinetic and isotherm models were evaluated by the linear correlation coefficient (R^2).

RESULTS AND DISCUSSION

Characterization of the adsorbent

Figure 2a shows the XRD diffraction pattern of ZnFe-NC. All diffraction peaks of the nanocomposite are in good agreement with the standard diffraction pattern of cubic spinel-structured zinc ferrite $ZnFe_2O_4$ (JCPDS card no: 22-1012) (Fig. 2b). No other impurity peaks were detected indicating the purity of the synthesized sample. The average crystallite size of ZnFe-NC calculated by Scherrer equation was 11 nm.

Figure 3 shows the SEM image of the synthesized ZnFe-NC. SEM analysis indicates the presence of agglomerates of small particles. In addition, SEM image clearly shows that nanoparticles of ZnFe-NC have irregular spherical shape. Figure 4a and 4b show the HRTEM image of

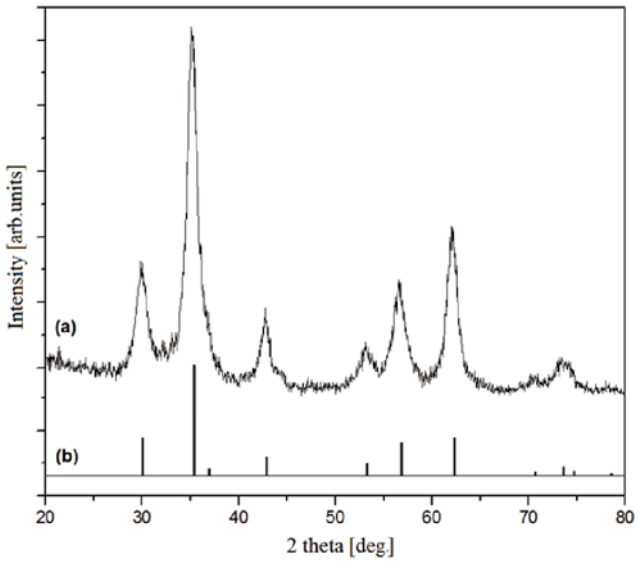

Figure 2. XRD patterns of ZnFe-NC (a) and standard $ZnFe_2O_4$ (JCPDS 22-1012) (b)

Figure 3. SEM image of ZnFe-NC. Inset: magnetic separation of ZnFe-NC from the aqueous solution by permanent magnet

ZnFe-NC nanoparticles and particle size distribution of nanoparticles, respectively. It shows that the size of the obtained nanoparticles is in the range of 4–13 nm. The magnetic properties of the material were presented elsewhere[31]. The magnetic measurements showed the superparamagnetic behavior of ZnFe-NC nanoparticles, which allowed their magnetic separation from water.

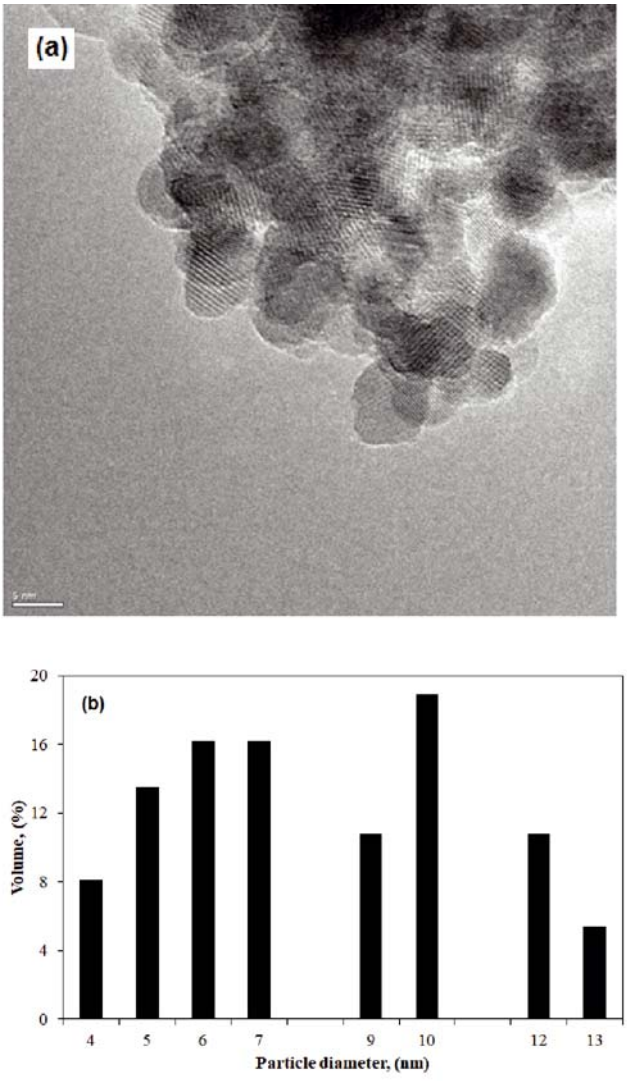

Figure 4. HRTEM image of ZnFe-NC (a) and particle size distribution (b)

As shown in inset of Figure 3, the magnetic separation performance of the composite was tested by placing a magnet near the glass bottle. ZnFe-NC was attracted toward the magnet in a short period.

Figure 5 presents the FTIR spectra of $ZnFe_2O_4$. Two main broad metal-oxygen bands are seen in the FTIR spectra of all spinels, and ferrites in particular. The highest one, ν_1, is generally observed in the range 600–500 cm^{-1}, and it corresponds to intrinsic stretching vibrations of the metal at the tetrahedral site, $M_{tetra} \leftrightarrow O$, whereas the ν_2 lowest band is usually observed in the range 430–385 cm^{-1}, is assigned to octahedralmetal stretching, $M_{octa} \leftrightarrow O$[32]. The band, observed at 562 cm^{-1} for $ZnFe_2O_4$ can be assigned to tetrahedral Zn^{2+} stretching, ν_1, and the band observed at 410 cm^{-1} involves the Fe^{3+} vibration at the octahedral site, ν_2. The peaks at 1387, 1060, and 845 cm^{-1} present in the IR spectrum of $ZnFe_2O_4$ can be assigned to the vibration of NO_3^- group trapped in the prepared sample[33–35]. The bands at 1545 cm^{-1} and 3415 cm^{-1} can be attributed to the O-H stretching vibration and H-O-H bending vibration of the free or absorber water molecules[36].

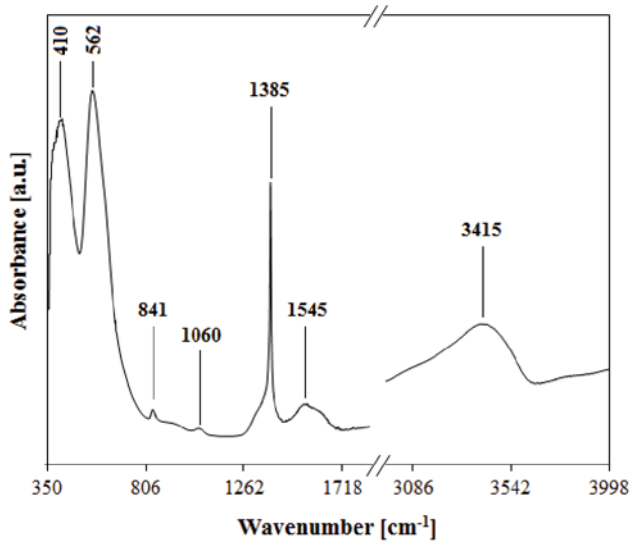

Figure 5. FTIR spectra of ZnFe-NC

The specific surface area calculated with the BET equation was 139 m^2g^{-1}. The point of zero charge is the pH value at which the amount of acidic and basic functional groups is equal. In Figure 10 the plot of $\Delta pH = pH_{initial} - pH_{final}$ versus $pH_{initial}$ is showed. Based on this plot, the pHpzc of ZnFe-NC was found to be 8.5.

Effect of initial dye concentration

Figure 6 shows the effect of the initial dye concentration on the amount of RB adsorbed by ZnFe-NC at pH 7.0 and at 20°C. As shown, the adsorption increases with increasing initial dye concentration. When the initial RB concentration varied from 5 to 25 mg L^{-1}, the adsorption capacity increased from 5.02 to 9.83 mg g^{-1}.

To examine the mechanism of the adsorption process, three kinetic models including the pseudo-first-order, pseudo-second-order and intraparticle diffusion model, are used to test experimental data. The pseudo-first-order kinetic model (Eq. 3) and pseudo-second-order kinetic model (Eq. 4) are given by the following equations[37]:

$$\ln(q_e - q_t) = \ln q_e - k_1 t \quad (3)$$

$$\frac{t}{q_t} = \frac{1}{k_2 q_e^2} + \frac{1}{q_e} t \quad (4)$$

where k_1 (min^{-1}) is the pseudo-first-order rate constant adsorption, t (min) time, k_2 (g mg^{-1} min^{-1}) is the pseudo-second-order rate constant adsorption. Values of k_1 and q_e were calculated from the linear plots of $\ln(q_e - q_t)$ versus t (Fig. 7a). Values of k_2 and q_e were calculated from the slope and intercept of the linear plots obtained by graphical representation of t/q_t versus t (Fig. 7b).

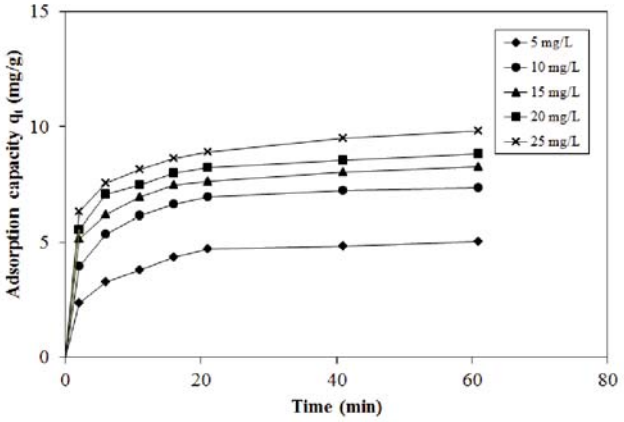

Figure 6. The effect of initial dye concentration on adsorption capacity of the RB onto ZnFe-NC (experimental conditions: T = 20°C, pH = 7)

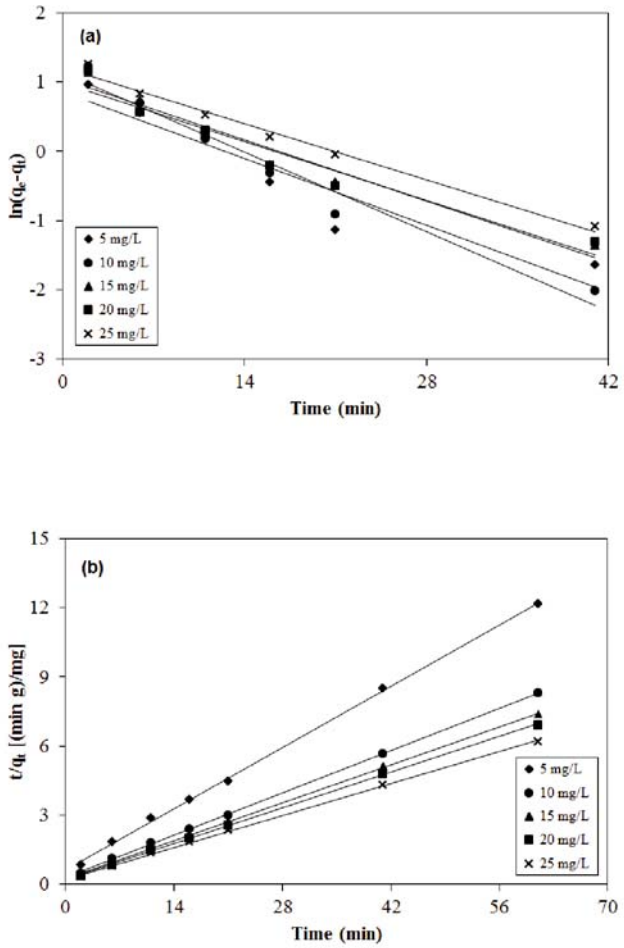

Figure 7. Pseudo-first-order (a) and pseudo-second-order (b) kinetics for adsorption of the RB onto ZnFe-NC (experimental conditions: T = 20°C, pH = 7)

Kinetic constants obtained by linear regression for the models and the correlation coefficients R^2 were summarized in in Table 1. Although the R^2 values for the pseudo-first-order kinetic model were relatively high ($R^2 = 0.8974 \div 0.9861$) for initial concentration of 5–25 mg L^{-1}, the experimental $q_{e,exp}$ values did not agree with the calculated $q_{e,cal}$ values obtained from the linear plots. The correlation coefficient values R^2 for the pseudo--second-order kinetic model were almost equal to unity ($R^2 = 0.9990 \div 0.9998$) for all initial dye concentrations studied. Moreover the calculated $q_{e,cal}$ values agree with the experimental data $q_{e,exp}$. This reveals that the adsorption of RB onto ZnFe-NC follows the pseudo--second-order kinetic model. The similar phenomena have also been observed in adsorption of Rhodamine B from aqueous solution onto sodium montmorillonite[13], onto walnut shells[16] and onto graphene nanocomposite[17].

The intraparticle diffusion equation is expressed as[38]:

$$q_t = k_p t^{0.5} + C \tag{5}$$

where C (mg g^{-1}) is the boundary layer thickness and k_p (mg g^{-1} $min^{-0.5}$) is the intraparticle diffusion rate constant. If the regression of q_t versus $t^{0.5}$ is linear and passes through the origin, then intraparticle diffusion is the sole rate-limiting step. From Figure 8, which shows the plot of the intraparticle diffusion model, it was noted that two linear portions occur. The first sharper portion is the mass transfer of solute molecules from the bulk solution to the adsorbent surface. The second portion is the gradual adsorption stage, wherein intraparticle diffusion is rate limiting. As can be seen from Figure 8, the linear portions of the intraparticle region do not pass through origin in any of the plots indicating that while intraparticle diffusion is involved, it is not the only rate-limiting mechanism. The k_p value increases with increasing the initial dye concentration (Table 1), which reveals that the rate of adsorption is governed by the diffusion of adsorbed dye within the pores of adsorbent[39]. Additionally, the constant C increases with increasing the initial dye concentration indicating the increase in thickness of the boundary layer and decrease of the chance of the external mass transfer and hence increase of the chance of internal mass transfer[40].

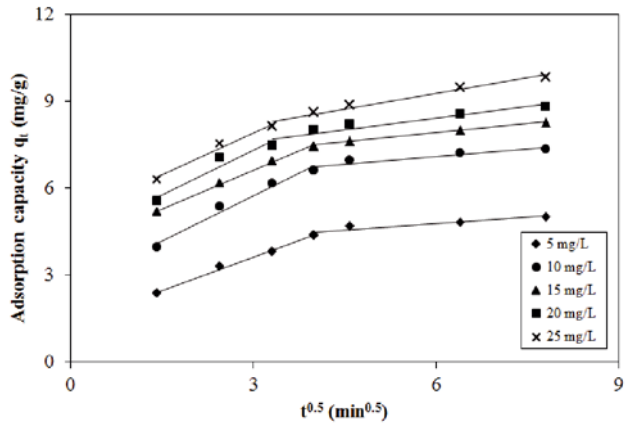

Figure 8. Intraparticle diffusion model of adsorption RB onto ZnFe-NC (experimental conditions: T = 20°C, pH = 7)

Adsorption isotherms

Langmuir and Freundlich isotherm models were employed to investigate the adsorption process. The application of the Langmuir isotherm model is based on monolayer coverage of adsorbent surfaces by the adsorbate. The Freundlich isotherm model is an empirical equation based on the multilayer adsorption of an adsorbate onto heterogeneous surfaces.

The linear form of Langmuir isotherm model is given by the following equation[41]:

$$\frac{C_e}{q_e} = \frac{1}{Q_0 b} + \frac{C_e}{Q_0} \tag{6}$$

where Q_O (mg g^{-1}) is the monolayer adsorption capacity and b (L mg^{-1}) is a constant related to energy of adsorption. The values of Q_O and b were calculated from the slope and intercept of the linear plot C_e/q_e versus C_e (Fig. 9a). The essential characteristics of the Langmuir isotherm can be expressed in terms of dimensionless equilibrium parameter (R_L), which is defined by the following equation:

$$R_L = \frac{1}{1 + bC_O} \tag{7}$$

where b (L mg^{-1}) is the Langmuir constant and C_O (mg L^{-1}) is the highest initial concentration of the adsorbate. The value of R_L indicates the type of the isotherm to be either unfavorable ($R_L > 1$), linear ($R_L = 1$), favorable ($0 < R_L < 1$) or irreversible ($R_L = 0$).

The Freundlich adsorption isotherm model is expressed by equation as[42]:

$$q_e = K_F C_e^{\frac{1}{n}} \tag{8}$$

The linearized-integral form of the Freundlich equation is represented by:

$$\ln q_e = \ln K_F + \left(\frac{1}{n}\right) \ln C_e \tag{9}$$

where K_F (mg g^{-1}(L $mg^{-1})^{1/n}$) and n are Freundlich constants, which represent adsorption capacity and adsorption strength, respectively. The values of K_F and n were calculated from the slope and intercept of the linear plot ln q_e versus ln C_e (Fig. 9b). The value of

Table 1. Comparison of the pseudo-first-order, pseudo-second-order and the intraparticle diffusion models for different initial concentrations of RB at 20°C

C_o [mg L^{-1}]	$q_{e,exp}$ [mg g^{-1}]	Pseudo-first-order model			Pseudo-second-order model			Intraparticle diffusion model		
		k_1 [min^{-1}]	$q_{e,cal}$ [mg g^{-1}]	R^2	k_2 [g mg^{-1} min^{-1}]	$q_{e,cal}$ [mg g^{-1}]	R^2	k_p [mg g^{-1} $min^{-0.5}$]	C [mg g^{-1}]	R^2
5	5.02	0.0687	2.36	0.8974	0.0582	5.26	0.9990	0.1448	3.90	0.8692
10	7.36	0.0821	3.13	0.9646	0.0567	7.63	0.9998	0.1765	6.03	0.8945
15	8.28	0.0631	2.85	0.9585	0.0551	8.51	0.9995	0.2133	6.64	0.9921
20	8.81	0.0606	2.68	0.9387	0.0595	9.02	0.9996	0.2678	6.81	0.9009
25	9.83	0.0579	3.38	0.9861	0.0438	10.10	0.9991	0.3617	7.10	0.9670

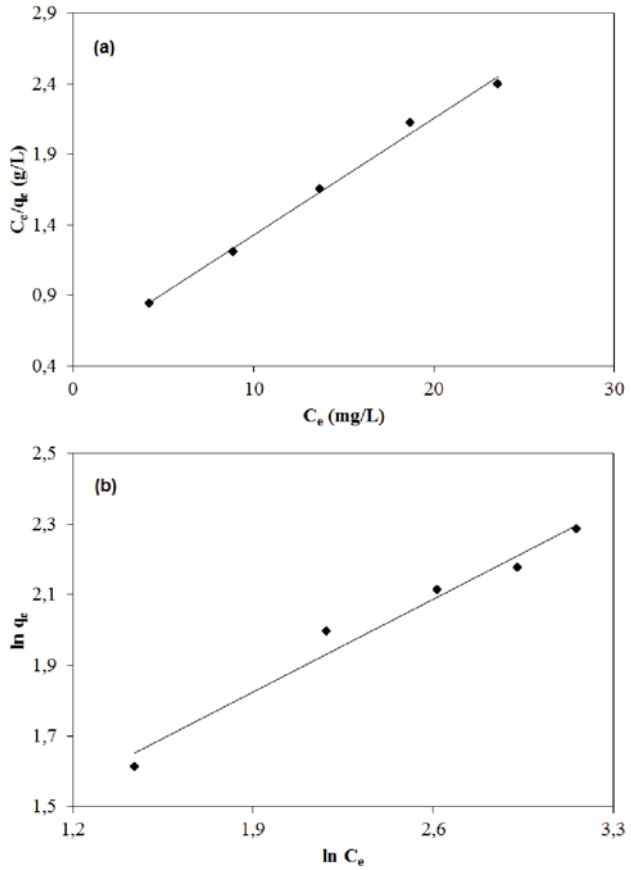

Figure 9. Langmuir (a) and Freundlich (b) isotherms for RB adsorption onto ZnFe-NC

n ranging from 1 to 10 indicated that the adsorption process is favourable.

Table 2 summarizes all the constants and correlation coefficient R^2 values obtained from the isotherm models. The correlation coefficient value for the Langmuir isotherm was greater than for the Freundlich isotherm. This showed that the Langmuir isotherm model fitted the experimental data better than the Freundlich model. The R_L value was in the range of 0–1, meanwhile, n for Freundlich isotherm was greater than 1, indicating on favourable adsorption of RB onto ZnFe-NC under conditions applied in this study. The maximum adsorption capacity Q_O determined from the Langmuir isotherm was 12.1 mg g^{-1}. Table 3 lists the comparison of maximum monolayer adsorption capacity of RB onto various adsorbents.

Effect of initial pH

The effect of initial pH on adsorption capacity at equilibrium of RB was studied by varying the pH of the dye solution from 3.4 to 11.1 for an initial concentration of 5 mg L^{-1} and at 20° (Fig. 10). Additionally, in Figure 10, the plot of ΔpH versus $pH_{initial}$ is showed.

Based on this plot, the pHpzc of ZnFe-NC was found to be 8.5, at which the surface of adsorbent has zero net charge (neutral). At pH<pHpzc, ZnFe-NC surface is positively charged, favoring the adsorption of anionic dyes due to increased of electrostatic interactions whereas at pH>pHpzc ZnFe-NC surface is negatively charged, favoring the adsorption of cationic dyes. At pH values lower than 4, the RB ions are of cationic and monomeric molecular form (Fig. 1a). Thus, at pH 3.4 (5.31 mg g^{-1}), a significantly high electrostatic repulsion force exist between the positively charged surface of the adsorbent and positively charged RB. As the pH of the dye solution increases, the number of positively charged sites on ZnFe-NC decreases and the number of negatively charged sites increases. Therefore, when the pH was increased from 3.4 to 4.4, the adsorption capacity at equilibrium of RB increased from 5.31 to 6.02 mg g^{-1}. However, as it can be seen in Figure 10 with a further increase of pH from 4.4 to 11.1, the adsorption capacity of RB decreased from 6.02 to 3.20 mg g^{-1}. At pH values higher than 4.4, the decrease of adsorption capacity may be due to the aggregation of RB to form a larger molecular form as dimer. When solution pH increased above 4.0, the carboxyl group gets ionized and the zwitterionic form of RB is formed (Fig. 1b). The zwitterionic form of RB may increase the aggregation of RB to form a bigger molecular form (dimer) and become unable to enter into the pore. The greater aggregation of the zwitterionic form is due to the attractive electrostatic interactions between the carboxyl and xanthene groups of the monomers[14]. When the pH is higher than 7.0, excessive OH^- ions compete with R-COO^- in binding with R-N^+ and the aggregation of RB decreases[37]. Thus, when the initial pH of the dye solution increases from 7.0 to 11.1 more molecules of RB exist mainly in the anionic form. At pHpzc (8.5) the number of positive and negative surface functional groups is equal and the positively charged sites on the ZnFe-NC favor the adsorption of anionic form of RB due to the electrostatic attraction. However, when the pH of the dye solution increases above 8.5, the numer of positively charged sites on surface of the adsorbent decreases and increase the repulsive electrostatic forces

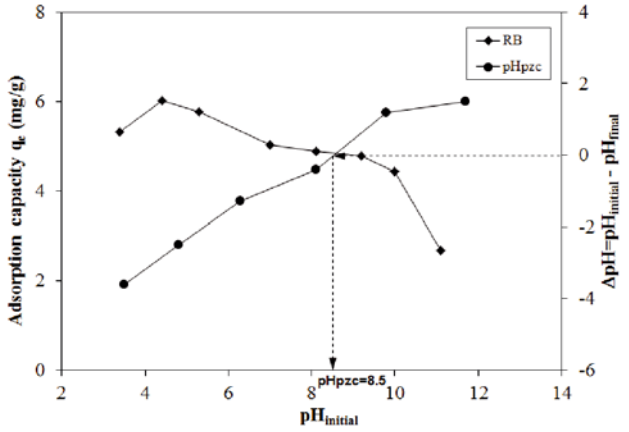

Figure 10. The pHpzc of ZnFe-NC and the effect of initial pH of dye solution on adsorption capacity of the RB onto ZnFe-NC (experimental conditions: CORB = 5 mg L^{-1}, T = 20°C)

Table 2. Langmuir and Freundlich parameters for the adsorption of the RB onto ZnFe_NC at 20°C

Langmuir isotherm				Freundlich isotherm		
Q_O [mg g^{-1}]	b [L mg^{-1}]	R_L	R^2	K_F [(mg g^{-1})(L mg^{-1})$^{1/n}$]	n	R^2
12.1	0.166	0.19	0.9941	3.03	2.66	0.9727

Table 3. Comparison of the maximum monolayer adsorption of RB onto various adsorbents

Adsorbent	Q_O [mg g^{-1}]	Ref.
Titania-silica	0.11	43
Zeolite MCM-22	1.11	44
Australian natural zeolite	2.12	45
Walnut shells	2.292	16
Tannic acid in Leacril	2.7	46
Coal ash	2.86	47
Cellulosic waste orange peel	3.23	48
Coffee ground powder	5.26	49
Bentonite	7.7	50
Luffa cylindrical	9.9	51
ZnFe-NC	12.1	This study
Sago waste derived activated carbon	16.1	52
Anaerobic sludge	19.52	53
Cellulose-based wastes	20.6	54
Duoline C-20 resin	28.571	55
Sodium montmorillonite	42.19	13
Kaolinite	46.1	18
Perlite	67.935	19
Jute stick powder	87.7	56
Graphene	201.207	17
BPH activated carbon	263.9	14
Activated carbon derived from scrap tires	307.2	37
Rice husk-based porous carbons	383.4	57

between the negatively charged surface of the adsorbent and negatively charged dye molecules, which does not favor the adsorption of RB onto ZnFe-NC.

Effect of temperature

Figure 11a shows the relationship between the temperature and the adsorption capacity of RB onto ZnFe-NC.

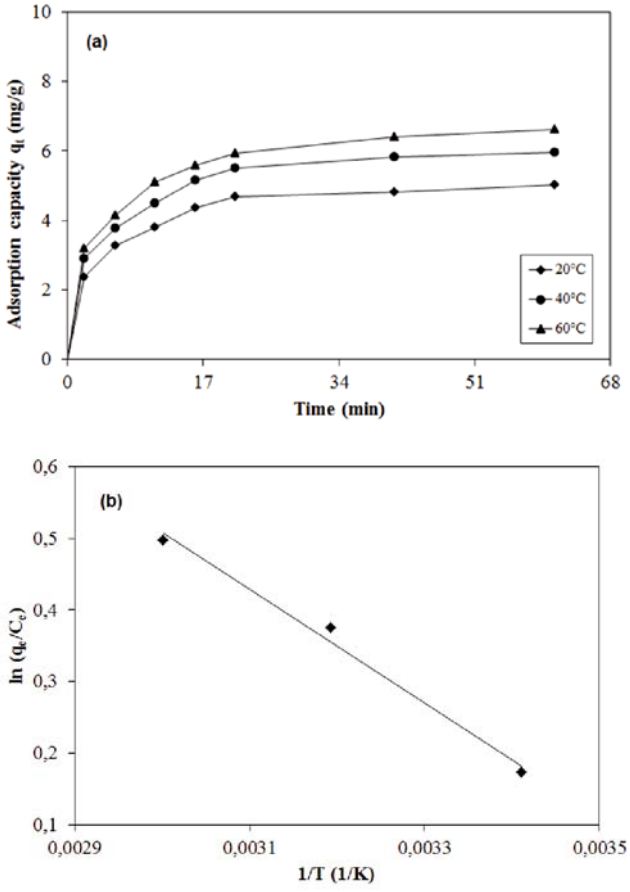

Figure 11. a) Effect of temperature on adsorption of the RB onto ZnFe-NC (experimental conditions: CORB = 5 mg L^{-1}, pH = 7). (b) Van't Hoff plot for the adsorption of the RB onto ZnFe-NC

With increasing temperature from 20°C to 60°C, the adsorption capacity increased from 5.02 to 6.62 mg g^{-1}, indicating that the adsorption process is endothermic. Thermodynamic parameters such as a change in free energy (ΔG^O), enthalpy (ΔH^O) and entropy (ΔS^O), were determined using following equations:

$$\ln K_a = \frac{\Delta S^o}{R} - \frac{\Delta H^o}{R \cdot T} \tag{10}$$

$$K_a = \frac{q_e}{C_e} \tag{11}$$

$$\Delta G^o = -RT \ln K_a \tag{12}$$

where T (K) is the solution temperature, K_a is the adsorption equilibrium constant. Enthalpy (ΔH^O) and entropy (ΔS^O) were calculated from the slope and intercept from the plot of ln (q_e/C_e) versus 1/T (Fig. 11b). The value of Gibbs free energy (ΔG^O) was calculated using Eq. 12. Thermodynamic parameters are given in Table 4. The positive value of ΔH^O confirmed that the adsorption process was endothermic. The positive value of ΔS^O showed the increasing randomness at the solid-solution interface during the adsorption of the RB onto ZnFe-NC. The ΔG^O values were negative at all of the test temperatures, confirming that the adsorption of RB onto ZnFe-NC was spontaneous and thermodynamically favorable. The extent of enthalpy ΔH^O gave an idea about a type of adsorption which is mainly physical or chemical. Typically, the adsorption enthalpy of physisorption is lower than 40 kJ mol^{-1}, while that of chemisorption may reach values between 40 and 120 kJ mol^{-1} [58]. In this study ΔH^O the value was in the range of physisorption, indicating on the physical nature of the adsorption. Generally, the change in free energy for physisorption is between –20 and 0 kJ mol^{-1} and for chemisorption is in a range of –80 to –400 kJ mol^{-1} [59]. The values of ΔG^O are within the range of –20 to 0 kJ mol^{-1}, indicating on physisorption as predominant mechanism of the adsorption process. Similar results were also observed in the adsorption of Rhodamine B onto kaolinite[18], adsorption

Table 4. Thermodynamic parameters for the adsorption of the RB onto ZnFe-NC

ΔH^O [kJ mol^{-1}]	ΔS^O [J mol^{-1} K^{-1}]	ΔG^O at temperature [^{O}C] [kJ mol^{-1}]			R^2
6.60	24.0	20	40	60	0.9894
		−0.42	− 0.97	−1.38	

of Rhodamine B onto walnut shells[16] and onto activated carbon prepared from bagasse pith[14].

CONCLUSIONS

Removal of Rhodamine B (RB) from aqueous solution using magnetic $ZnFe_2O_4$ nanocomposite (ZnFe-NC) was investigated. The nanocomposite was synthesized using microwave assisted hydrothermal method. The prepared adsorbent can be easily separated from the medium after adsorption using an external magnetic field.

The experimental data were analyzed using Langmuir and Freundlich isotherm models. The adsorption isotherm data were best fitted to the Langmuir isotherm model with an maximum adsorption capacity of 12.1 mg g^{-1}, which indicated monolayer sorption onto the homogeneous surface of the ZnFe-NC. The kinetic study of RB adsorption on ZnFe-NC was performed based on pseudo-first-order, pseudo-second-order and intraparticle diffusion kinetic models. The data indicated that the adsorption kinetics followed the pseudo-second-order rate with intraparticle diffusion as one of the rate determining steps. According to the thermodynamic parameters, the adsorption process of RB onto ZnFe-NC nanocomposite was spontaneous and endothermic.

LITERATURE CITED

1. Arora, S. (2014). Textile Dyes: It's Impact on Environment and its Treatment. *J. Bioremed. Biodeg.* 5(3), 1. http://dx.doi.org/10.4172/2155-6199.1000e146.

2. Chen, X., Xue, Z., Yao, Y., Wang, W., Zhu, F. & Hong, C. (2012). Oxidation Degradation of Rhodamine B in Aqueous by UV/$S_2O_8^{2-}$ Treatment System. *Int. J. Photoenergy.* 2012, 1–5. http://dx.doi.org/10.1155/2012/754691.

3. Moghaddam, S.S., Moghaddam, M.R.A. & Arami, M. (2010). Coagulation/flocculation process for dye removal using sludge from water treatment plant: Optimization through response surface methodology. *J. Hazard. Mater.* 175(1–3), 651–657. https://doi.org/10.1016/j.jhazmat.2009.10.058.

4. Gadekar, M.R., Ahammed Civil Engineering Department, S V National Institute of Technology (2016). Coagulation/flocculation process for dye removal using water treatment residuals: modelling through artificial neural networks. *Desalin. Water Treat.* 57(55), 26392–26400. http://dx.doi.org/10.1080/19443994.2016.1165150.

5. Mohammadi, N., Khani, H., Gupta, V.K., Amereh, E. & Agarwal, S. (2011). Adsorption process of methyl orange dye onto mesoporous carbon material–kinetic and thermodynamic studies. *J. Colloid Interface Sci.* 362(2), 457–462. https://doi.org/10.1016/j.jcis.2011.06.067.

6. Gupta, V.K., Kumar, R., Nayak, A., Saleh, T.A. & Barakat, M.A. (2013). Adsorptive removal of dyes from aqueous solution onto carbon nanotubes: a review. *Adv. Colloid Interface Sci.* 193–194, 24–34. DOI:10.1016/j.cis.2013.03.003.

7. Salem, I.A. & El-Maazawi, M.S. (2000). Kinetics and mechanism of color removal of methylene blue with hydrogen peroxide catalysed by some supported alumina surfaces. *Chemosphere* 41, 1173–1180. https://doi.org/10.1016/S0045-6535(00)00009-6.

8. Masoumbeigi, H. & Rezaee, A. (2015). Removal of Methylene Blue (MB) dye from synthetic wastewater using UV/H_2O_2 advanced oxidation process. J. Health Policy Sustain. Health 2(1), 160–166.

9. Gupta, V.K., Jain, R., Mittal, A., Saleh, T.A., Nayak, A., Agarwal, S. & Sikarwar, S. (2012). Photo-catalytic degradation of toxic dye amaranth on TiO2/UV in aqueous suspensions. *Mater. Sci. Eng. C.* 32(1), 12–17. https://doi.org/10.1016/j.msec.2011.08.018.

10. Saravanan, R., Karthikeyan, S., Gupta, V.K., Sekaran, G., Narayanan, V. & Stephen, A. (2013). Enhanced photocatalytic activity of ZnO/CuO nanocomposite for the degradation of textile dye on visible light illumination. *Mater. Sci. Eng. C.* 33, 91–98. https://doi.org/10.1016/j.msec.2012.08.011.

11. Rashidi, H.R, Sulaiman, N.M.N., Hashim, N.A., Hassan, C.R.C. & Ramli, M.R. (2015). Synthetic reactive dye wastewater treatment by using nano-membrane filtration. *Desalin. Water Treat.* 55(1), 86–95. http://dx.doi.org/10.1080/19443994.2014.912964.

12. Majewska-Nowak, K. & Kawiecka-Skowron, J. (2011). Ceramic membrane behaviour in anionic dye removal by ultrafiltration. *Desalin. Water Treat.* 34, 367–373. DOI:10/5004/dwt.2011.2806.

13. Selvam, P.P., Preethi, S., Basakaralingam, P., Thinakaran, N., Sivasamy, A. & Sivanesan, S. (2008). Removal of rhodamine B from aqueous solution by adsorption onto sodium montmorillonite. *J. Hazard. Mater.* 155, 39–44. DOI: 10.1016/j.jhazmat.2007.11.025.

14. Gad, H.M.H. & El-Sayed, A.A. (2009). Activated carbon from agricultural by-products for the removal of Rhodamine-B from aqueous solution. *J. Hazard. Mater.* 168, 1070–1081. DOI: 10.1016/j.jhazmat.2009.02.155.

15. Huang, J.H., Huang, K.L., Liu, S.Q., Wang, A.T. & Yan, C. (2008). Adsorption of Rhodamine B and methyl orange on a hypercrosslinked polymeric adsorbent in aqueous solution. *Colloids Surf. A Physicochem. Eng. Asp.* 330, 55–61. http://dx.doi.org/10.1016/j.colsurfa.2008.07.050.

16. Shah, J., Rasul Jan, M., Haq, A. & Khan, Y. (2013). Removal of Rhodamine B from aqueous solutions and wastewater by walnut shells: kinetics, equilibrium and thermodynamics studies. *Front. Chem. Sci. Eng.* 7(4), 428–436. DOI: 10.1007/s11705-013-1358-x.

17. Liu, K., Li, H., Wang, Y., Gou, X. & Duan, Y. (2015). Adsorption and removal of rhodamine B from aqueous solution by tannic acid functionalized graphene. *Colloids and Surfaces A: Physicochem. Eng. Asp.* 477, 35–41. http://dx.doi.org/10.1016/j.colsurfa.2015.03.048.

18. Khan, T.A., Dahiya, S. & Ali, I. (2012). Use of kaolinite as adsorbent: Equilibrium, dynamics and thermodynamic studies on the adsorption of Rhodamine B from aqueous solution. *Appl. Clay Sci.* 69, 58–66. http://dx.doi.org/10.1016/j.clay.2012.09.001.

19. Vijayakumar, G., Tamilarasan, R. & Dharmendirakumar, M. (2012). Adsorption, Kinetic, Equilibrium and Thermodynamic studies on the removal of basic dye Rhodamine-B from aqueous solution by the use of natural adsorbent perlite. *J. Mater. Environ. Sci.* 3(1), 157–170. ISSN: 2028-2508.

20. Zhang, Z. & Kong, J. (2011). Novel magnetic Fe_3O_4@C nanoparticles as adsorbents for removal of organic dyes from aqueous solution. *J. Hazard. Mater.* 193, 325–329. DOI: 10.1016/j.jhazmat.2011.07.033.

21. Xie, Y., Qian, D., Wu, D. & Ma, X. (2011). Magnetic halloysite nanotubes/iron oxide composites for the adsorption of dyes. *Chem. Eng. J.* 168, 959–963. DOI: 10.1016/j.cej.2011.02.031.

22. Singh, K.P., Gupta, S., Singh, A.K. & Sinha, S. (2011). Optimizing adsorption of crystal violet dye from water by magnetic nanocomposite using response surface modeling approach. *J. Hazard. Mater.* 186, 1462–1473. DOI: 10.1016/j.jhazmat.2010.12.032.

23. Madrakian, T., Afkhami, A., Ahmadi, M. & Bagheri, H. (2011). Removal of some cationic dyes from aqueous solutions using magnetic-modified multi-walled carbon nanotubes. *J. Hazard. Mater.* 196, 109–114. DOI: 10.1016/j.jhazmat.2011.08.078.

24. Mahmoodi, N.M. (2013). Magnetic ferrite nanoparticle-alginate composite: synthesis, characterization and binary system dye removal. *J. Taiwan Inst. Chem. Eng.* 44, 322–330. DOI: 10.1016/j.jtice.2012.11.014.

25. Gao, H., Zhao, S., Cheng, X., Wang, X. & Zheng, L. (2013). Removal of anionic azo dyes from aqueous solution using magnetic polymer multi-wall carbon nanotube nanocomposite as adsorbent. *Chem. Eng. J.* 223, 84–90. DOI: 10.1016/j.cej.2013.03.004.

26. Yao, Y., Miao, S., Liu, S., Ma, L.P., Sun, H. & Wang, S. (2012). Synthesis, characterization,and adsorption properties of magnetic Fe_3O_4@graphene nanocomposite. *Chem. Eng. J.* 184, 326–332. DOI: 10.1016/j.cej.2011.12.017.

27. Wu, Q., Feng, C., Wang, C. & Wang, Z. (2013). A facile one-pot solvothermal method to produce superparamagnetic graphene-Fe_3O_4 nanocomposite and its application in the removal of dye from aqueous solution. *Colloids Surf. B: Biointerf.* 101, 210–214. DOI: 10.1016/j.colsurfb.2012.05.036.

28. Wang, L., Li, J., Wang, Y., Zhao, L. & Jiang, Q. (2012). Adsorption capability for Congo red on nanocrystalline MFe_2O_4 (M = Mn, Fe, Co, Ni) spinel ferrites. *Chem. Eng. J.* 181–182, 72–79. DOI: 10.1016/j.cej.2011.10.088.

29. Ai, L., Zhou, Y. & Jiang, J. (2011). Removal of methylene blue from aqueous solution by montmorillonite/$CoFe_2O_4$ composite with magnetic separation performance. *Desalination* 266, 72–77. DOI: 10.1016/j.desal.2010.08.004.

30. Lopez-Ramon, M.V., Stoeckli, F., Moreno-Castilla, C. & Carrasco-Marin F. (1999). On the characterization of acidic and basic surface sites on carbons by various techniques. *Carbon* 37, 1215–1221. DOI: 10.1016/S0008-6223(98)00317-0.

31. Kuryliszyn-Kudelska, I., Hadzic, B., Sibera, D., Romcevic, M., Romcevic, N., Narkiewicz, U. & Dobrowolski, W. (2011). Dynamic magnetic properties of ZnO nanocrystals incorporating Fe. *J. Alloys Compd.* 509, 3756–3759. DOI: 10.1016/j.jallcom.2011.01.004.

32. Koseoglu, Y., Baykal, A., Gozuak, F. & Kavas, H. (2009). Structural and magnetic properties of $Co_xZn_{1-x}Fe_2O_4$ nanocrystals synthesized by microwave method. *Polyhedron* 28, 2887–2892. DOI: 10.1016/j.poly.2009.06.061.

33. Weinzierl, D., Touraud, D., Lecker, A., Pfitzner, A. & Kunz, W. (2008). Controlled preparation of hollow zinc oxide microspheres from aqueous solution using hexamethylenetetramine and cysteine. *Mater. Res. Bull.* 43, 62–67. DOI: 10.1016/j.materresbull.2007.02.017.

34. Varshney, D., Verma, K. & Kumar, A. (2011). Structural and vibrational properties of $Zn_xMn_{1-x}Fe_2O_4$ (x = 0.0, 0.25, 0.50, 0.75, 1.0) mixed ferrites. *Mater. Chem. Phys.* 131, 413–419. DOI: 10.1016/j.matchemphys.2011.09.066.

35. Mouallem-Bahout, M., Bertrand, S. & Pena, O. (2005). Synthesis and characterization of $Zn_{1-x}Ni_xFe_2O_4$ spinels prepared by a citrate precursor. *J. Solid State Chem.* 178, 1080–1086. DOI: 10.1016/j.jssc.2005.01.009.

36. Sharifi, I. & Shokrollahi, H. (2012). Nanostructural, magnetic and Mossbauer studies of nanosized $Co_{1-x}Zn_xFe_2O_4$ synthesized by co-precipitation. *J. Magn. Magn. Mater.* 324, 2397–2403. http://dx.doi.org/10.1016/j.jmmm.2012.03.008.

37. Li, L., Liu, S. & Zhu, T. (2010). Application of activated carbon derived from scrap tires for adsorption of Rhodamine B. *J. Environ. Sci.* 22(8), 1273–1280. DOI: 10.1016/S1001-0742(09)60250-3.

38. Weber, W.J. & Morris, J.C. (1963). Kinetics of adsorption on carbon from solution. *J. Sanit. Eng. Div.* 89, 31–60.

39. Baskaran, P. K., Venkatraman, B. R., Hema, M. & Arivoli, S. (2010). Adsorption studies of copper ion by low cost activated carbon. *J. Chem. Pharm. Res.* 2(5), 642–655.

40. Santhi, T., Manonmani, S., Vasantha, V.S. & Chang, Y.T. (2011). A new alternative adsorbent for the removal of cationic dyes from aqueous solution. *Arabian J. Chem.* DOI: 10.1016/j.arabjc.2011.06.004.

41. Langmuir, I. (1918). The adsorption of gases on plane surfaces of glass, mica and platinum. *J. Am. Chem. Soc.* 40, 1361–1403.

42. Freundlich, H. (1906). Concerning adsorption in solutions. *Z. Phys. Chemie.* 57, 385–470.

43. Messina, P.V. & Schulz, P. (2006). Adsorption of reactive dyes on titanic-silica mesoporous materials. *J. Colloid Interface Sci.* 299, 305–320. DOI: 10.1016/j.jcis.2006.01.039.

44. Wang, S., Li, H. & Xu, L. (2006). Application of zeolite MCM-22 for basic dye removal from waste water. *J. Colloid Interface Sci.* 295, 71–78. DOI: 10.1016/j.jcis.2005.08.006.

45. Wang, S. & Zhu, Z.H. (2006). Characterization and environmental application of an Australian natural zeolite for basic dye removal from solution. *J. Hazard. Mater.* 136, 946–952. DOI: 10.1016/j.jhazmat.2006.01.038.

46. Martin, E.G. & Jimenez, M.E. (2005). Influence of tannic acid in Leacril/Rhodamine B system: Thermodynamics aspects. *Colloids Surf. A Physicochem. Eng. Asp.* 270/271, 93–101. http://dx.doi.org/10.1016/j.colsurfa.2005.05.047.

47. Wang, S., Soudi, M., Li, L. & Zhu Z.H. (2006). Coal ash conversion into effective adsorbent for removal of heavy metals and dyes from waste water. *J. Hazard. Mater.* 133, 243–251. DOI: 10.1016/j.jhazmat.2005.10.034.

48. Namasivayam, C., Muniasamy, N., Gayathri, K., Rani, M. & Ranganathan, K.(1996). Removal of dyes from aqueous solution by cellulosic waste orange peel. *Bioresour. Technol*. 57, 37–43. http://dx.doi.org/10.1016/0960-8524(96)00044-2.

49. Shen, K. & Gondal, M.A. (2013). Removal of hazardous Rhodamine dye from water by adsorption onto exhausted coffee ground. *J. Saudi Chem. Soc.* http://dx.doi.org/10.1016/j.jscs.2013.11.005.

50. Tahir, S.S. & Rauf, N. (2006). Removal of cationic dye from aqueous solutions by adsorption onto bentonite clay. *Chemosphere* 63, 1842–1848.

51. Altinisik, A., Gur, E. & Seki, Y. (2010). A natural sorbent, Luffa cylindrica for the removal of a model basic dye. *J. Hazard. Mater.* 179, 658–664. DOI: 10.1016/j.jhazmat.2010.03.053.

52. Kadirvelu, K., Karthika, C., Vennilamani, N. & Pattabhi, S. (2005). Activated carbon from industrial solid waste as an adsorbent for the removal of Rhodamine-B from aqueous solution: Kinetic and equilibrium studies. *Chemosphere* 60(8), 1009–1017. DOI: 10.1016/j.chemosphere.2005.01.047.

53. Wang, Y., Mu, Y., Zhao, Q.B. & Yu, H.Q. (2006). Isotherms, kinetics and thermodynamics of dye biosorption by anaerobic sludge. *Sep. Purif. Technol.* 50, 1–7. DOI: 10.1016/j.seppur.2005.10.012.

54. Annadurai, G., Juang, R.S. & Lee, D.J. (2002). Use of cellulose-based wastes for adsorption of dyes from aqueous solutions. *J. Hazard. Mater.* 92, 263–274. DOI: 10.1016/S0304-3894(02)00017-1.

55. Al-Rashed, S.M. & Al-Gaid, A.A. (2012). Kinetic and thermodynamic studies on the adsorption behavior of Rhodamine B dye on Duolite C-20 resin. *J. Saudi Chem. Soc.* 16, 209–215. http://dx.doi.org/10.1016/j.jscs.2011.01.002.

56. Panda, G.C., Das, S.K. & Guha, A.K. (2009). Jute stick powder as a potential biomass for the removal of Congo Red and Rhodamine B from their aqueous solution. *J. Hazard. Mater.* 164(1), 374–379. DOI: 10.1016/j.jhazmat.2008.08.015.

57. Guo, Y.P., Zhao, J.Z., Zhang, H., Yang, S.F., Qi, J.R., Wang, Z.C. & Xu, H. (2005). Use of rice husk-based porous carbon for adsorption of Rhodamine B from aqueous solu-

tions. *Dyes Pigm.* 66(2), 123–128. http://dx.doi.org/10.1016/j.dyepig.2004.09.014.

58. Chatterjee, S. & Woo, S.H. (2009). The removal of nitrate from aqueous solutions by chitosan hydrogel beads. *J. Hazard. Mater.* 164, 1012–1018. DOI: 10.1016/j.jhazmat.2008.09.001.

59. Crini, G. & Badot, P.M. (2010). *Sorption processes and pollution. Conventional and non-conventional sorbents for pollutant removal from wastewaters.* Presses universitaires de Franche-Comté, France.